SPE 36916

Thermally Induced Fracturing: Analysis of a Field Case in North Sea

P. Charlez, SPE, Total, and P. Lemonnier, SPE, IFP, and C. Ruffet, Stilog, and M.J. Boutéca, SPE, IFP, and C. Tan, Altran

This paper was prepared for presentation at the 1996 SPE European Petroleum Conference held in Milan, Italy, 22-24 October 1996.

Abstract

Thermally Induced Fracturing (TIF) is often observed on injection wells. In this paper a well documented TIF case is presented and analysed. A numerical model is first presented where waterflooding is computed in two steps. In the first step, radial flow is considered and stress changes are computed. Depending on rock characteristics and flow rate the thermal effect (stress decrease) dominates over the pressure effect (stress increase). In the second step, as soon as the fracturing criterion is reached, the model automatically switches to a coupled two-phase flow option where a PKN type fracture has been incorporated. The main features of the model are summarized. To validate the model a field case has been analyzed where bottom hole pressure and temperature have been recorded. From field data it is shown that in the initial stage the height of the fracture varies and is thus different from the pay zone thickness. Use of Perkins and Gonzalez solution together with Prats formula allows to assess height and length evolution of the fracture. From this information, a mean fracture height can be assessed for the test duration. It is then shown that the pressure profile versus time is well given back using the numerical model, thus confirming the previous estimation of fracture dimensions.

Introduction

Waterflooding is still today the most common oil recovery method. It is aimed at improving recovery together with increasing production rate.

Apart from any recovery process, injection of a cold fluid into a warmer reservoir induces thermal stresses, the main effect of which is to relax the hoop stress component $\sigma_{\theta\theta}$ over a certain distance. Indeed, the typical hoop stress profile (Fig.1) around an injection well shows two distinct parts [1,2]. In the section of the reservoir which has already been cooled, the thermal hoop stress is negative. Consequently, the total hoop stress is relaxed compared to its original value σ_h. This relaxation is, however, modulated by the hydraulic component (variation of stress associated with variation of pore pressure), which, depending on the voidage (balance between injection at the considered well and production from adjacent wells), can be either positive or negative. By contrast, in the zone which has not yet been affected by cooling, and for obvious equilibrium reasons, the hoop stress is greater than the original minor geostatic stress σ_h. Between these two zones, a very thin transition with a very steep stress gradient prevails.

If hoop stress $\sigma_{\theta\theta}$ (initially equal to σ_h) relaxes below the injection pressure P_{inj}, a hydraulic fracture will initiate and then propagate until the transition zone (which we will call *"stress wall"* for obvious reasons) in the vicinity of which it stops. The temperature via the thermal stress thus acts as a propagation regulator. In waterflooding, the resultant back stresses (hydraulic and thermal) can no more be neglected as in classical hydraulic fracturing.

Modelling of Thermal Induced Fracturing (T.I.F.) was initiated during the mid eighties by Perkins and Gonzales [3]. In their paper, they assume that thermal conductivity can be neglected with respect to convection (in practice, this is almost always the case). Consequently, temperature is a step function and the reservoir area can be divided into a cold zone (at fluid temperature T_f) and a hot, undisturbed zone at reservoir temperature T_R. Furthermore, as they assume a constant injection flow rate Q, the volume of the cooled zone can easily be calculated at any time t writing the energy balance between injected and received heat. As the fracture propagates, the cold zone initially radial lengthens parallel to the fracture direction. This suggests approximating the cooled region by an ellipsis confocal to the fracture direction (the fracture tip merges with the foci of the ellipsis - Fig. 2). The half-axes a_0 and b_0 are given by the following formulae:

$$a_0 = \frac{L}{2}\left(\sqrt{X} + \frac{1}{\sqrt{X}}\right) \qquad b_0 = \frac{L}{2}\left(\sqrt{X} - \frac{1}{\sqrt{X}}\right)$$

$$\text{with} \quad X = \frac{Q\,t\,C_f}{C_r}\frac{2}{\pi L^2 h} + \frac{1}{2}\sqrt{\left(\frac{4}{\pi L^2 h}\frac{QtC_f}{C_r}\right)^2 + 4} \tag{1}$$

where h and L are respectively fracture height and length C_f and C_r are fluid and rock volumetric heat ($J/°C.m^3$). Perkins & Gonzales propose an analytical solution for thermoelastic hoop stresses (elliptic inclusion of finite thickness h at temperature T_f centered in an infinite block at temperature T_R):

$$\frac{\Delta\sigma_{\theta\theta}^{ther}(1-\nu)}{\alpha E\left(T_R - T_f\right)} = -\frac{(b_0/a_0)}{1+(b_0/a_0)} - \left[\frac{1}{1+(b_0/a_0)}\right] * \frac{1}{1+0.5\left[1.45\left(\frac{h}{2b_0}\right)^{0.9} + 0.35\left(\frac{h}{2b_0}\right)^{2}\right]\left[1+\left(\frac{b_0}{a_0}\right)^{0.774}\right]} \tag{2}$$

where α, E and ν are respectively the thermal expansion coefficient, the Young's modulus and the Poisson's ratio of the rock. For thick reservoirs ($b_0 << h$), the dimensionless thermal stress decreases versus fracture length. By contrast, for sufficiently thin reservoirs, thermal stress increases when the fracture propagates (Fig. 3).

Although very useful for a first estimate of the fracture length, Perkins and Gonzalez's solution does not allow to reproduce complex injection schemes.

Since the mid 80's, many authors have addressed the numerical modelling of thermal induced fracturing [4,5,6]. In these models, diffusion equations are generally uncoupled and back stresses are calculated using the Goodier and Timoshenko potentials method [7]. Most of these models also assume that the temperature in the fracture is constant and equal to that of the injected fluid. Given the very long injection times (several years) the Carter type law (which has the major advantage of decoupling the fracture from the porous medium) can no longer be used, as it is only valid for short term operations. Consequently, pore pressure must be calculated from a two-dimensional Darcy's law.

However, these models do not take into account the initial state (pressure, temperature and stress) induced by a matricial radial injection prior to fracture opening.

Within the framework of ARTEP[1] a numerical model including an initial radial injection phase has been developed. This model is briefly described in the next section.

[1]Research association between IFP, ELF and TOTAL.

The HYDFRAC model

The HYDFRAC model[8] is based on a 3-D two-phase thermal reservoir model for heterogeneous, anisotropic and compressible porous media. At any time, for a fracture of given length L in which one injects a cold fluid at temperature T_w and for a given flow rate Q, the reservoir module computes pressure and temperature fields together with fluid saturation (Fig. 4). Once pore pressure and temperature are known everywhere in the domain, hydraulic and thermal back stresses $\Delta\sigma_h^{hyd}$ and $\Delta\sigma_h^{ther}$ are computed along the fracture using Goodier and Timoshenko's potentials. For fracture propagation, one assumes a PKN geometry[9] (fracture of constant height h, elliptical vertical sections in plane state of strain). Consequently, fracture width is given by the following equation:

$$w(x,t) = \frac{1-\nu}{G} h\left\{p_f(x,t) - \sigma(x,t)\right\}$$
$$\sigma = \sigma_h + \Delta\sigma_h^{hyd} + \Delta\sigma_h^{ther} \tag{3}$$

where G and ν are respectively the shear modulus and Poisson's ratio. According to Eq. (3), in order to propagate the fracture by an extra length element Δx, the stress must be sufficiently relaxed on this element (Fig. 4). The hydraulic boundary conditions are either pressure or flow conditions at the wellbore and pressure at the external boundary or flow rate at a production well. In the latter case a five spot pattern is assumed:

$$q(x=0,y=0,t) = Q(t) \quad \text{or} \quad p(x=0,y=0,t) = p_w(t)$$
$$p(x,y=0,t) = p_f \quad x \le L$$
$$p(x,y=\infty,t) = p_R \quad \forall x \quad \text{or} \quad q(x_p,y_p,t) = q_p(t) \tag{4}$$

where the subscript p stands for production.

Example of propagation modulated by a moving stress wall

The results of a 285 days simulation in a 2mD reservoir are presented on Fig. 5. Considering injection conditions ($\sigma_{\theta\theta}$ drops quickly below the injection pressure), the fracture initiates after only a few days. As pointed on Fig. 5b, the stress perpendicular to the fracture plane is relaxed compared to its initial value (equal to 40MPa) over a distance which is more or less equal to the cooled length. With propagation $\sigma_{\theta\theta}$ continually decreases (3 MPa at the well between 25 days and 285 days). The poroelastic effect (which has a tendency to increase $\sigma_{\theta\theta}$ in the cooled zone) is only visible on the first curve (25 days). Beyond the stress wall, as for circular geometry, the static equilibrium imposes a stress jump which far exceeds the initial geostatic stress value σ_h (equal to 40 MPa).

In so far as the average stress level in the cooled zone decreases with time, propagation pressure (Fig. 6) drops by

several MPa during the considered injection period (carried out at a constant flow rate).

This result is in opposition with that found in traditional fracturing (for a PKN type geometry, propagation pressure always increases versus fracture length). After 285 days, the fracture (h=62m) reaches 37m. Although clearly controlled by the stress wall, the fracture is opened over a distance smaller than the thermal radius.

Waterflood shut-in

Very often, injection conditions do not remain constant during the life of an injection well. In particular, injection can be stopped during several days. In the case described below we consider three injection phases: constant flow rate (510 m^3/d) during 100 days, shut-in during 10 days (flow rate=0) and finally a new injection phase at 510 m^3/d.

In response to shut-in the fracture instantaneously closes and the pressure drops to its initial value (Fig. 7). However, shut in of the well only slightly affects the thermal distribution: thermal conduction which is the only thermal process affecting temperature during shut-in is not able to warm up the reservoir. Consequently, when injection begins again, the fracture immediately re-opens over its total length (that existing before shut-in Fig. 7). During the post shut-in phase, the fracture propagates identically as if no shut-in had occurred. Waterflooding shut-in is not therefore a limitation to thermal induced fracturing.

Field example : the Alwyn field (North-Sea)

The Alwyn field lies to the East of the Shetland Islands in the English North Sea. The reservoir (called Brent) in which two main sandy levels can be identified (Tarbet and Ness) is located below 3200 meters TVD. The Tarbet itself is divided into three sub-levels: T1, T2, T3. 95% of the injected water is squeezed in the T3 (divided itself into an upper and a lower part). For this reason, we will assume in what follows that only T3 is affected by thermal fracturing. Its thickness is estimated at 46 m. The formation permeability (deduced from build-up tests carried out prior to injection) is estimated at 43 mD.

Initiation of a thermal induced fracture during a short term injection test

The five day test shown on Fig. 8 is a remarkable example of TIF. The well temperature (both BHP and BHT are measured during the test), initially equal to 90°C (reservoir temperature is 100°C), decreases slowly with time until it stabilises at about 30°. The initial injection phase (plateau at 40M^3/day/MPa - Fig. 8a) remains purely matricial. After about 25 hours, a sharp increase in injectivity is observed (the temperature is then equal to 50°C - Fig. 8c), clearly connected to the initiation of a thermal fracture. The injection pressure (Fig. 8b), initially 54.5 MPa (matricial injection pressure), quickly drops as soon as the fracture opens and stabilises at approximately 52 MPa.

Impact of reservoir pressure on long-term propagation

The long term (over several years) pore pressure evolution plays a role which is at least as important as the temperature. The pore pressure around an injection well does in fact evolve considerably during the field life. Depending on the voidage (difference between injected and produced volumes), it may either increase or decrease. The reservoir pressure evolution in the drainage area of an Alwyn injection well is shown on Fig. 9[2]. For the first three years, pressure decreases continuously, then from 1990, it increases due to the injection itself.

As already pointed in the introduction, these continuous variations in pressure cause a substantial modification of geostatic stresses [10,11]. On Fig. 9, bottom hole pressure (assumed to be equal to fracture propagation pressure) is calculated from surface data and pressure drop in the tubing. A remarkable correlation between the BHP and reservoir pressure is observed. Depending on the voidage, fracturing pressure may either increase or decrease. This perfectly reversible phenomenon confirms the poroelastic rheology of the rock.

Application of P&G's solution and HYDFRAC model on the short term injection test

The analytical solution of Perkins & Gonzales not being able to consider the radial phase and the injection history, the data have to be averaged during a single fracturing phase. Coming back to the injection test described in Fig. 8, the fracturing phase starts after 1,500 min. Consequently, instead of considering a matricial injection phase (approximately 400 m^3/day during 1,500 min.) followed by a fracturing phase (approximately 800m^3/day for 4,500 min.), the overall volume (some 2750m^3) is averaged at constant flow rate (equal to 880m^3/day) during 4,500 min.

As far as temperature is concerned, it is assumed that injection is implemented with a mean ΔT equal to 70°C. The initial stress σ_h is accurately measured (57.7 MPa) through good fitting between hydraulic minifrac results and laboratory tests (Differential Strain Curve Analysis [12,13]). The elastic parameters are obtained from core tests (E=25800MPa, ν=0.15). Volumetric heat for rock and fluid are respectively taken equal to 2.710^6J/m^3.°C and 4.210^6J/m^3.°C. However, two important variables remain little known : fracture height h and thermal expansion coefficient α.

As the fracture does not initiate over the whole layer thickness (46 m), it seems therefore more realistic to assume pseudo-radial propagation, assuming that at each time step, the fracture length is equal to its half-height (h=2L). For the thermal expansion coefficient, laboratory core measurements[13] give 4.10^{-5}/°C a value rather high for such a sandstone. Assuming that the calculated propagation pressure is equal to σ_h minus $\Delta\sigma_{\theta\theta}$ [calculated by equation (2)] we first try at each time step to fit the field BHP by adapting the

[2]These results are obtained from reservoir simulations

fracture dimensions. Then in a second phase, we check whether the estimated lengths are compatible with the measured injectivity index. The hydraulic stress (due to pore pressure variations) is neglected in this analytical approach.

The results of two sets of calculations are shown on Fig. 10. They differ by the thermal expansion coefficient which is respectively equal to 4.10^{-5}/°C (laboratory test value) and $1.5.10^{-5}$/°C. Fig. 10a shows that the Perkins & Gonzales solution provides a perfect fitting between the pressure curves in both cases. However, the fracture length (equal to half its height) required to fit the pressure is greater for the highest thermal expansion coefficient (Fig. 10b). After 4,500 minutes, it reaches 15.5 m for the highest value, less than 11 m in the other case. To calculate the injectivity index corresponding to a given fracture length, one uses the classical Prats's formula[14]. Considering the length/height ratio and an infinite fracture conductivity, Prats's formula is written (in terms of injectivity index).

$$II = \frac{4\pi k L}{\mu \ln\left[L/2R_d\right]} \qquad (5)$$

k, μ and R_d being respectively the rock permeability and the fluid viscosity (assumed one-phase flow). The drainage radius R_d being estimated at 500 m, fluid viscosity at 1 Cp and the rock permeability at 43 mD (value obtained from production tests), the injectivity index can then be calculated for each length and compared to the field value. Comparison between field data and calculated injectivities are presented on Fig. 11. Results show that Prats's model reproduces very well the field data for the smallest thermal expansion coefficient. However, for 4.10^{-5}/°C (core test value), the calculated injectivity index strongly overestimates field data.

We illustrate hereafter the use of the HYDFRAC model on the field case detailed above. In the light of the Perkins and Gonzales analysis, during this test the fracture propagates radially. To simulate the test with the HYDFRAC model (which assumes a PKN geometry and is not normally able to simulate such a radial propagation) an average fracture height equal to 12m is assumed. The purpose of the calculation is to get back the correct bottom hole pressure when imposing the injection history of Fig. 12.

As observed on Fig. 13, during the fracturing phase of the test, the calculated pressure fits quite well the field data. At the end of the test, the fracture length reaches 8 m, a value comparable to that observed with P&G (10 m).

Conclusions

1. Three major parameters govern the propagation of a thermal induced fracture: bottom hole temperature, reservoir pressure and injection rate.

2. The prime driving parameter is obviously temperature. Cooled zone extension which increases continuously with time, defines the theoretical maximum length of the thermal fracture. Depending on the daily flow rate (which can vary considerably following operational constraints) and reservoir permeability, the fracture will be opened over a distance of between zero and the maximum cooled length.

3. Reservoir pressure strongly governs fracture propagation pressure. If the reservoir pressure (due to a negative voidage) remains constant or drops continuously with time, the injectivity is maintained while the bottom hole pressure decreases. By contrast, if fluid balance leads to a reservoir pressure increase, the resulting poroelastic stress is opposed to the driving thermal stress. In that case, maintenance of injectivity (corresponding to an open fracture length) generally requires an increase of the bottom hole pressure.

4. It has been shown that in the initial stage, the fracture height varies and is thus different from the pay zone thickness.

5. A TIF numerical model which couples a thermal reservoir model with PKN fracture propagation has been presented. It allows to take into account complex injection and production schemes. Use of this model with height input taken from a previous analytical estimation, restitutes the pressure profile versus time, thus confirming the analytical estimation of the mean fracture height for the test duration and validating the model.

6. Future developments of the model will include integration of damage laws[15] and fracture height variation.

Acknowledgments

The authors gratefully acknowledge the support of members of ARTEP, an association of the French petroleum companies. The authors also thank F. Hage-Chehade for valuable discussion and for his contribution in the development of the model.

References

1. Perkins T.K. and Gonzales J.A. (1984) "Change in Earth Stresses Around a Wellbore Caused by Radially Symmetrical Pressure Temperature Gradients," SPEJ p 129-140.

2. Morales R.H., Abou-Sayed A.S. and Jones A.H. (1985) "Detection of formation fracture in a waterflooding experiment," SPE 13747.

3. Perkins T.K. and Gonzales J.A. (1985) "The effect of thermoelastic stress on injection well fracturing," SPE 11332.

4. Dikken B.J. and Niko H. (1987) "Waterflood induced fractures: a simulation study of their propagation and effects on waterflood sweep efficiency," SPE 16551.

5. Clifford P.J., Berry P.J. and Hongren Gu (1990) "Modelling the vertical containment of injection well thermal fractures," SPE 20741.

6. Settari A. and Warren G.M. (1994) "Simulation and field analysis of waterflood induced fracturing," SPE/ISRM 28081.

7. Timoshenko S.P. and Goodier J.N. (1970) "*Theory of Elasticity*," Mc Graw Hill.

8. Hage-Chehade F., Boutéca M. , Charlez P., Detienne J.L. and Tan C.H. (1995) "Modélisation numérique de propagation de fracture dans un milieu thermoporoélastique," 12ème congrès français de mécanique.

9. Nordgren P. (1972) "Propagation of a vertical hydraulic fracture," SPEJ 306-314.

10. Charlez P.A. (1996) "Rock Mechanics Vol. II Petroleum applications," Ed. Technip In Press.

11. Teufel W.L., Rhett D.W and Farrell H.E. (1991 "Effect of reservoir depletion and pore pressure drawdown on in situ stresses and deformation of the Ekofisk field, North Sea," 32nd US Symposium Rock Mechanics as a multidisciplinary science, Norman A.A. Balkema.

12. Simmons G., Siegfried R.W. and Feves M. (1975) "Differential Strain Analysis : A new method of examining cracks in rocks," JGR 79 4383-85.

13. Hamamdjian C. (1989) "Détermination de l'état de contrainte dans les massifs rocheux à partir de l'étude de la microfissuration des roches," Thèse Ecole Centrale de Paris.

14. Prats M. "Effect of Vertical Fracture on Reservoir behaviour - Incompressible fluid case," SPEJ 105-118.

15. Roque C., Chauveteau G., Renard M., Thibault G., Boutéca M. and Rochon J. (1995) "Mechanisms of formation damage by retention of particles suspended in injection water," SPE 30110.

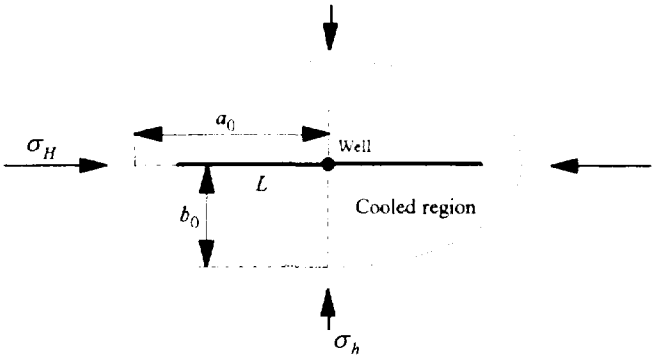

Fig. 2 - Shape of the cooled zone around a fractured borehole (after *Perkins and Gonzales, 1985*)

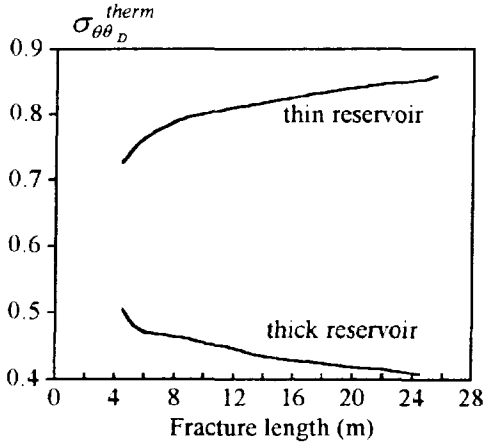

Fig. 3 - Evolution of dimensionless hoop thermal stress versus fractured length. Influence of formation thickness.

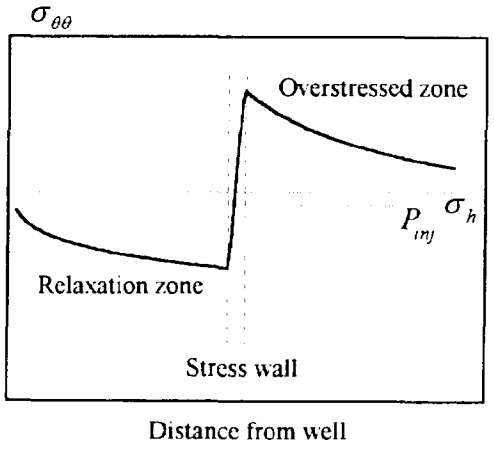

Fig. 1 - Hoop stress around an injection well

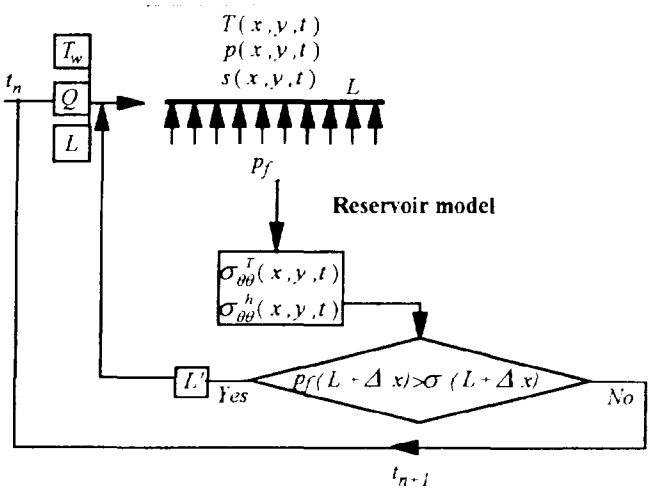

Fig. 4 - Simplified fracture propagation algorithm (boundary condition: constant flow rate)

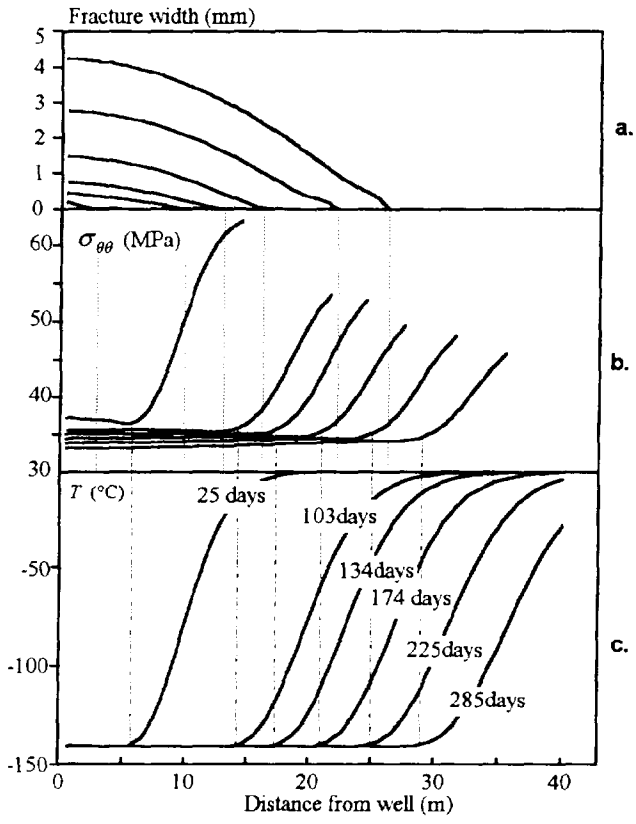

Fig. 5 - Simulation of thermal induced fracture propagation 285 days (HYDFRAC)

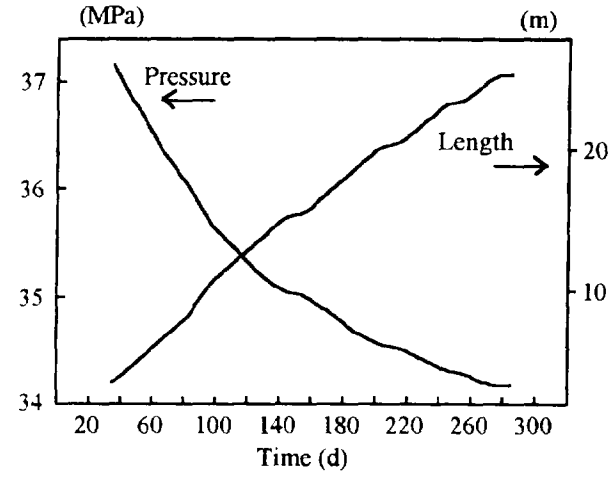

Fig. 6 - 2mD case. Length and pressure as a function of time.

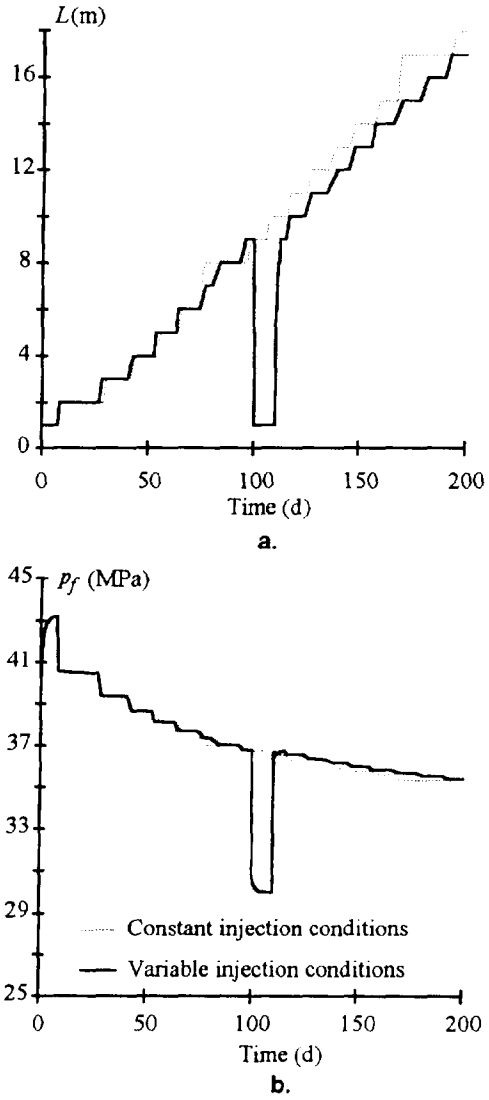

Fig. 7 - Effect of a waterflooding shut-in

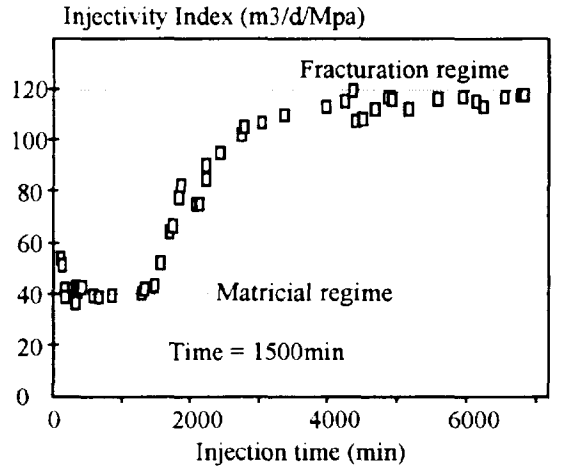

a.

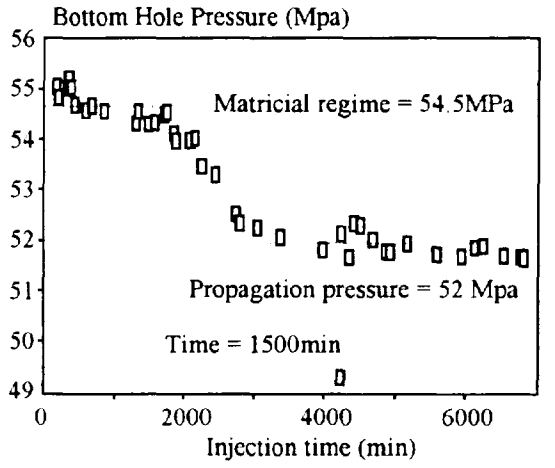

b.

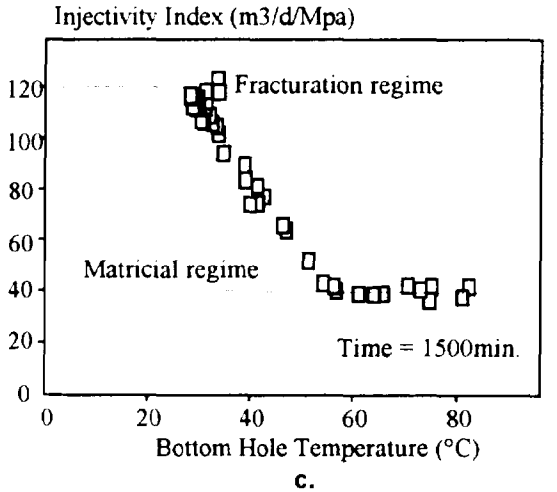

c.

Fig. 8 - Short term injectivity test.

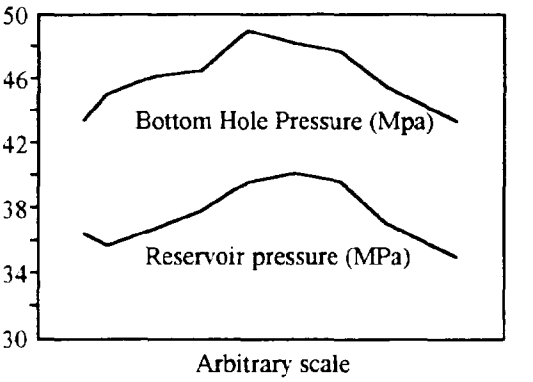

Fig. 9 Correlation between bottom hole and reservoir pressures

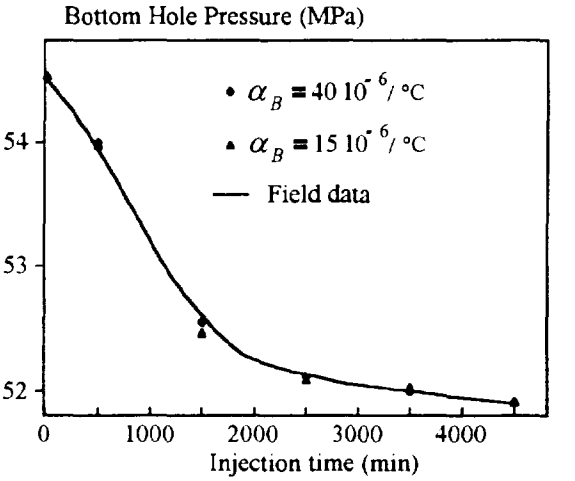

a.

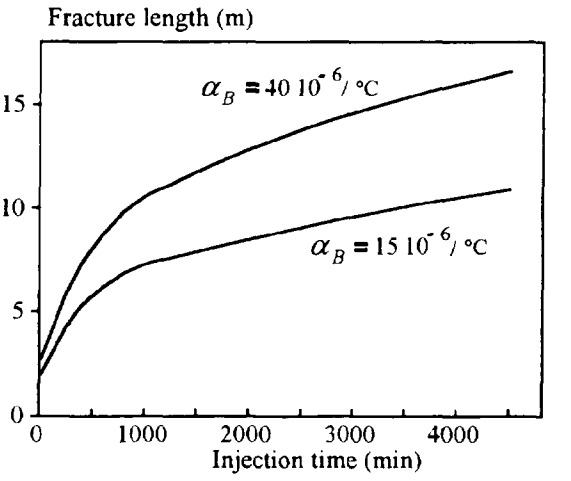

b.

Fig. 10 - Determination of fracture length for two different values of the thermal expansion coefficient

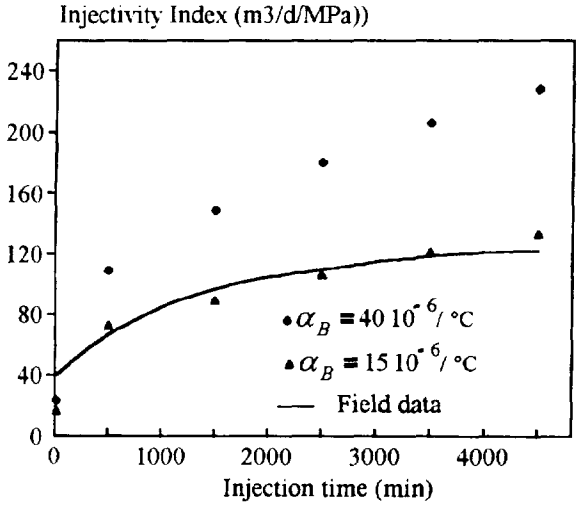

Fig. 11 - Comparison of field injectivity indices to those calculated using Prats's model.

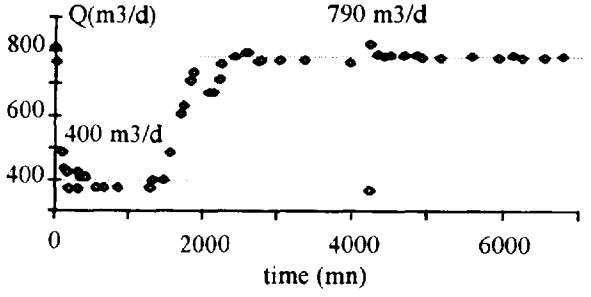

Fig. 12 - Field data used to simulate the short term injection test with the HYDFRAC model.

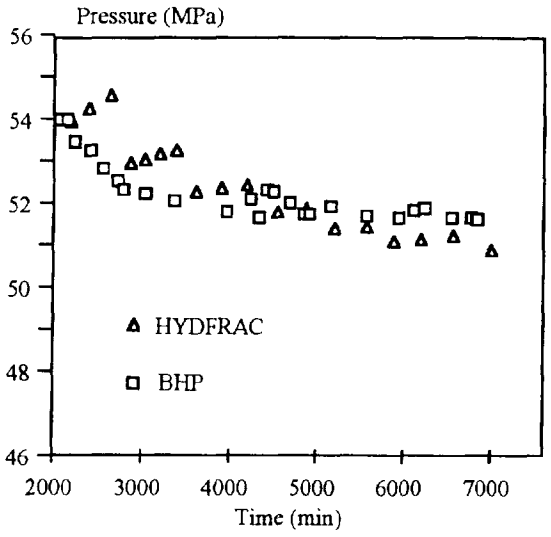

Fig. 13 - Comparison of measured and computed bottomhole pressures.